Theor Chem Acc (2005) 114: 189–199
DOI 10.1007/s00214-005-0660-1

REGULAR ARTICLE

N.R. Jena · P.C. Mishra

An ab initio and density functional study of microsolvation of carbon dioxide in water clusters and formation of carbonic acid

Received: 8 May 2004 / Accepted: 11 July 2004 / Published online: 28 May 2005

Abstract Geometry of the CO_2–H_2O complex and reaction barriers leading to the formation of H_2CO_3 were studied at the RHF/6-311++G**, MP2/6-311++G**, B3LYP/AUG-cc-pVDZ, B3LYP/AUG-cc-pVTZ, MP2/AUG-cc-pVDZ and CCD/AUG-cc-pVDZ levels of theory. The rotational barrier of the CO_2–H_2O complex and the reaction barrier leading to the formation of H_2CO_3–H_2O from CO_2–$(H_2O)_2$ were studied using the first three of the above-mentioned methods. Microsolvation of CO_2 in water clusters having upto eight water molecules was studied using the B3LYP/AUG-cc-pVDZ method. Various methods except MP2/AUG-cc-pVDZ predict the equilibrium structure of the CO_2–H_2O complex to be symmetric while the MP2/AUG-cc-pVDZ method predicts it to be unsymmetric. Formation of H_2CO_3 from CO_2–H_2O is strongly catalyzed by the presence of a second water molecule. Atomic orbitals are strongly rehybridized in going from the equilibrium structures of the CO_2–H_2O and CO_2–$(H_2O)_2$ complexes to the transition states involved in the formation of H_2CO_3 and H_2CO_3–H_2O, respectively, as shown by hybridization displacement charges.

Keywords Hydration of CO_2 · Rotational barrier · Reaction barrier · Carbonic acid · Hybridization displacement charge

1 Introduction

Intermolecular interaction between the CO_2 and H_2O molecules is of great interest due to its importance in different areas of science and technology, for example, biology, environment, oceanography and geology. CO_2 is involved in several biochemical reactions in living systems. It is present in human blood and is produced in a number of ways, for example, respiration, citric acid cycle, fatty acid synthesis and gluconeogenesis [1–3]. It is one of the main ingredients of photosynthesis and is frequently used in soft drinks [3,4]. As a green house gas, CO_2 absorbs infrared radiation emitted by the earth, which leads to increase in the environmental temperature. According to the current estimates, about 25% of CO_2 entering the earth's atmosphere is accumulated by oceans and its solubility in ocean water is very high [5,6].

On the basis of a matrix isolation infrared spectroscopic study, the CO_2–H_2O complex has been suggested to have a so-called T-shaped structure having no hydrogen bonding between the CO_2 and H_2O molecules [7]. A radio frequency and microwave spectroscopic study employing molecular beam electric resonance technique has also suggested the same structure for the CO_2–H_2O complex [8]. This structure of the CO_2–H_2O complex is planar conforming to the C_{2v} point group, where the hydrogen atoms point away from CO_2 [7–9]. In this complex, the barrier hindering rotation of H_2O with respect to CO_2 was experimentally found to be 0.9 ± 0.2 kcal/mol [8]. Jönsson et al. [9] calculated this rotational barrier and found it to be 1.3 kcal/mol, but there is no other theoretical study available so far in this context. The CO_2–H_2O complex has been described as one of van der Waals type [8–10] but the nature of bonding in this complex has not been properly investigated. The CO_2–$(H_2O)_2$ complex was studied using the pulsed molecular beam Fourier transform microwave spectroscopy, and it was suggested to be planar, cyclic [11]. In these studies, the rotational constants A, B and C are directly measured while geometries are derived using these constants along with some assumptions, for example, that of no change in the geometries of the individual molecules on complex formation. Validity of these assumptions and geometries of the complexes obtained on the basis of these assumptions need to be studied using rigorous quantum chemical calculations.

Several ab initio quantum chemical investigations have been carried out on the structures and stability of complexes of CO_2 with water molecules and formation of H_2CO_3 [12–18]. Most of the theoretical calculations support the geometries obtained experimentally using the above-mentioned approach. However, agreement between the calculated and experimentally observed rotational constants was not analyzed in the previous studies. Nguyen and Ha [14] studied

N.R. Jena · P.C. Mishra (✉)
Department of Physics, Banaras Hindu University,
Varanasi – 221 005 India
E-mail: pcmishra@bhu.ac.in

formation of carbonic acid starting with hydration of CO_2 by a water dimer employing the RHF/3-21G procedure and obtained the barrier height as 15.5 kcal/mol that is quite close to the experimental value (17.7 kcal/mol) [19]. The study of the same reaction barrier by Mertz [16] yielded its value as 40.45 kcal/mol at the RHF/6-31G** level and 32.17 kcal/mol at the MP2/6-31G** level, which indicates the importance of electron correlation in this context. Lewis and Glaser [18] from MP2(full) calculations employing the 6-31G*, 6-31G** and 6-311G** basis sets obtained the reaction barrier to be 31.69, 30.92 and 34.17 kcal/mol, respectively. Further, their single point MP4(full, SDTQ)/6-311G** and QCISD(T)/6-31G** calculations using the geometries obtained at the MP2 (full) level as mentioned above gave the reaction barrier as 35.67 and 31.76 kcal/mol, respectively [18]. It appears desirable to examine if searching the transition state using better basis sets than those used previously, for example, the correlation-consistent ones, along with a method that accounts for electron correlation adequately, would improve the agreement with experiment. A strong rehybridization of atomic orbitals of atoms involved in the reaction leading to the formation of H_2CO_3 at the transition state has been suggested in a previous investigation using atomic site-based point charges [18]. This interesting aspect deserves to be studied in more detail including atomic orbital hybridization in the treatment explicitly. A systematic study of microsolvation of CO_2 in water clusters of varying sizes using a method that takes care of electron correlation is missing. It would be interesting to examine if a solvation shell of water molecules around CO_2 would exist.

In view of the above reasons, we have studied the following aspects: (1) Geometries of the CO_2–$(H_2O)_n$, (n = 1, 2), complexes and modifications in the monomer geometries in the same have been studied, and agreement between the calculated and experimentally observed rotational constants analyzed, (2) Nature of bonding in the CO_2–$(H_2O)_n$, (n = 1–8), complexes have been investigated, (3) Ab initio and density functional methods that are known to treat electron correlation satisfactorily along with correlation-consistent and other basis sets were employed, and RHF calculations were also performed for the sake of comparison of results, particularly to examine the effects of electron correlation, (4) Rehybridization of atomic orbitals in going from equilibrium geometries of the CO_2–$(H_2O)_n$, (n = 1, 2) complexes to the corresponding transition states involved in the formation of H_2CO_3 and H_2CO_3–H_2O have been studied using hybridization displacement charges (HDC) [20–25] that are particularly suited for this purpose, and (5) A systematic study of microsolvation of CO_2 in water clusters consisting of upto eight water molecules have been carried out.

2 Computational methodology

The geometries of CO_2, H_2O and the CO_2–H_2O complex were optimized at the RHF/6-311++G**, MP2/6-311++G**, B3LYP/AUG-cc-pVDZ, B3LYP/AUG-cc-pVTZ, MP2/AUG-cc-pVDZ and CCD/AUG-cc-pVDZ levels of theory [26–30]. The reaction barrier heights leading to the formation of H_2CO_3 from the CO_2–H_2O complex were also investigated at all the above-mentioned levels of theory. The geometry of the CO_2–$(H_2O)_2$ complex was optimized at all the above-mentioned levels of theory, except CCD/AUG-cc-pVDZ. The rotational barrier of H_2O with respect to CO_2 in the CO_2–H_2O complex was studied at the RHF/6-311++G**, MP2/6-311++G** and B3LYP/AUG-cc-pVDZ levels of theory. Molecular electrostatic potential (MEP)-derived CHelpG point charges [31] located at the atomic sites were obtained for H_2O, CO_2 and the CO_2–H_2O complex. The reaction barrier leading to the formation of H_2CO_3–H_2O from the CO_2–$(H_2O)_2$ complex was studied employing the RHF/6-311++G**, MP2/6-311++G** and B3LYP/AUG-cc-pVDZ methods. Vibrational frequency analysis was carried out in all the cases where geometry optimization was performed, and zero-point energy (ZPE) corrections were made to the calculated rotational and reaction barrier energies. Complexation of CO_2 with a larger number of water molecules than two, upto eight, were studied using the B3LYP/AUG-cc-pVDZ method. The equilibrium structures of reactants and products as well as those of transition states were visualized using the GaussView (versions 2.1 and 3.09) program [32, 33]. All the calculations were performed employing the Windows versions of the Gaussian 94 [34], Gaussian 98 [35] and Gaussian 03 [36] programs. HDC [20–25] were computed using a software developed in our laboratory.

3 Results and discussions

3.1 Structure, stability and properties of the CO_2–H_2O complex

The optimized structure of the CO_2–H_2O complex is found to be planar at all the levels of theory employed here. Further, the optimized structure is symmetric, and so-called T-shaped (Fig. 1a) [7–9] at all the levels of theory except at MP2/AUG-cc-pVDZ where it is found to the unsymmetric (Fig. 1b). The experimental CO distance between the carbon atom of CO_2 and the oxygen of H_2O is 2.836 Å [8]. The differences of the various calculated CO distances obtained by different theoretical methods in the present work from this experimental value lie in the range 0.003–0.061 Å (Table 1). The CO distances obtained by the RHF/6-311++G** and B3LYP/AUG-cc-pVDZ methods are in particularly good agreement with the experimental value, while the CO distance obtained by the MP2/AUG-cc-pVDZ method is also fairly close to it. Since the CCD/AUG-cc-pVDZ method is the best among all those employed here in the sense of accounting for electron correlation, it is somewhat perplexing that the calculated value of the CO distance at this level is appreciably different from the experimental one, and it is close to the CO distance obtained in a previous RHF/6-31G** calculation by Zhang

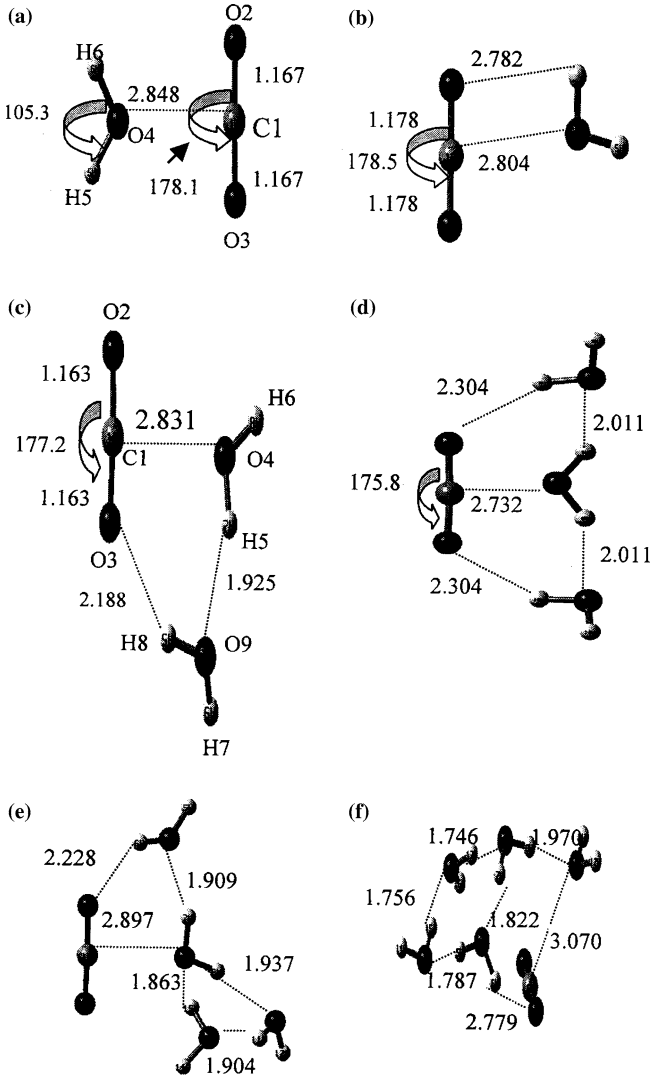

Fig. 1 Optimized structures of CO_2–$(H_2O)_n$, $n = 1$–5, complexes. The structure of **b** was optimized by the MP2/AUG-cc-pVDZ method while all the other structures were optimized by the B3LYP/AUG-cc-pVDZ method

and Shillady [37]. It shows that electron correlation plays a complex role in this case.

A comparison of the calculated and observed [8] dipole moments of the CO_2–H_2O complex show the error to be largest at the RHF/6-311++G** level and smallest at the MP2/AUG-cc-pVDZ level (Table 1). The various calculated binding energies of the CO_2–H_2O complex in the present work lie between ~ -0.08 and ~ -0.15 eV (Table 1). There is no experimental value of binding energy available for comparison with the calculated ones. The CO_2–H_2O binding has been described in the previous studies as one of van der Waals type [7–9]. To investigate the nature of binding in this complex, the following calculations were performed. The MEP-derived CHelpG charges on the various atoms of the CO_2–H_2O complex were obtained at the different levels of theory. These charges were used to calculate the interaction energy ($\Delta E1$) between CO_2 and H_2O in the CO_2–H_2O complex. Subsequently, the CHelpG point charges located at the atomic site in the complex were replaced by those in isolated CO_2 and H_2O molecules and the interaction energy ($\Delta E2$) was again calculated without changing the geometry of the complex. The interaction energies $\Delta E1$ and $\Delta E2$ so obtained are presented in Table 1. We find that the binding energies and interaction energies $\Delta E1$ and $\Delta E2$ obtained by different methods for the CO_2–H_2O complex are qualitatively similar. A further analysis of the CHelpG charges shows that there is no significant charge transfer between the two components of the complex. These results suggest that the CO_2–H_2O complex is mainly held by electrostatic interactions between the CO_2 and H_2O components and the contribution of van der Waals binding that would be related to polarization of charges in the two components is much smaller.

On CO_2–H_2O complex formation, the CO bond lengths of CO_2 and OH bond lengths of H_2O remain almost unchanged while the CO_2 molecule becomes somewhat bend from linearity, the bending angle lying in the range from $\sim 1.5^\circ$ to $\sim 2.3^\circ$. according to the different theoretical methods (Fig. 1a,b). Further the HOH bond angle of H_2O in the CO_2–H_2O complex is increased in comparison to that in an isolated H_2O molecule, the amounts of increase lying between $\sim 0.4^\circ$ and $\sim 1.0^\circ$ according to the different methods. Thus is due to formation of the CO_2–H_2O complex, geometrical parameters of the two constituents are modified by small amounts.

When the method employed was MP2/AUG-cc-pVDZ, the optimized structure of the CO_2–H_2O complex was found to be planar and unsymmetric, one OH bond of the water molecule being almost parallel to one of the CO bonds of CO_2 as shown in Fig. 1b. In order to be able to decipher whether the symmetric structure of Fig. 1a or the unsymmetric structure of Fig. 1b would be observed experimentally, we may use the basis of the agreement between the observed and calculated principal rotational constants presented in Table 2, since the experimental geometry is derived from these constants along with some assumptions. The calculated principal rotational constants A, B and C of CO_2–H_2O and CO_2–D_2O obtained at the MP2/AUG-cc-pVDZ level of theory are in a significantly better agreement (error $\sim$0.40%) with the experimental values due to Peterson and Klemperer [8] than those obtained at the other levels of theory (errors $\sim$1.3 to $\sim$2%) (Table 2). On the basis of this criterion, the observed structure of the CO_2–H_2O complex appears to be unsymmetric, as obtained by geometry optimization at the MP2/AUG-cc-pVDZ level (Fig. 1b) in the present study.

3.2 Structure, stability and properties of the CO_2–$(H_2O)_2$ complex

The values of the binding energy of the CO_2–$(H_2O)_2$complex per water molecule obtained at the different levels of theory are presented in Table 3. A comparison of these binding energies with those obtained for the CO_2–H_2O complex

Table 1 Binding energies per H_2O molecule, interaction energies ($\Delta E1$ and $\Delta E2$) between the CO_2 and H_2O molecules, $CO(H_2O)$ distances and dipole moments obtained by different methods for the CO_2–H_2O complex

Method/Basis set	Binding energy (eV)	Interaction energy (eV)		$CO(H_2O)$ (Å)[c]	Dipole moment (Debye)
		$\Delta E1$[a]	$\Delta E2$[b]		
Experiment[d]				2.836	1.852
RHF/6-311++G**	−0.121	−0.146	−0.151	2.833(symmetric)	2.477
B3LYP/AUG-cc-pVDZ	−0.084	−0.095	−0.104	2.848(symmetric)	2.213
B3LYP/AUG-cc-pVTZ	−0.077	−0.094	−0.103	2.869(symmetric)	2.207
MP2/6-311++G**	−0.146	−0.152	−0.167	2.775(symmetric)	2.406
MP2/AUG-cc-pVDZ	−0.129	−0.142	−0.143	2.804(unsymetric)	2.051
CCD/AUG-cc-pVDZ	−0.091	−0.133	−0.133	2.789(symmetric)	2.391
RHF/6-31G**[e]	−0.142			2.782	

[a]Values of interaction energy ($\Delta E1$) between CO_2 and H_2O were obtained by considering interaction of CHelpG point charges obtained in the CO_2–H_2O complex
[b]Values of interaction energy ($\Delta E2$) between CO_2 and H_2O were obtained by considering interaction of CHelpG point charges calculated for isolated CO_2 and H_2O molecules, the geometry remaining the same as that for $\Delta E1$
[c]The type of structure, that is, symmetric or unsymmetric as obtained at different levels of theory are given in parentheses
[d]From Ref. [8]
[e]From Ref. [37]

Table 2 Rotational constants for CO_2–H_2O, CO_2–D_2O, CO_2–$(H_2O)_2$ and CO_2–$(D_2O)_2$ complexes obtained by different methods

Method/Basis set	Rotational constants (MHz)[a]		
	A	B	C
CO_2–H_2O and CO_2–D_2O			
Experiment[b]	11506 (11222)	4674 (4216)	3304 (3049)
RHF/6-311++G**	11911 (11597)	4636 (4148)	3337 (3055)
B3LYP/AUG-cc-pVDZ	11293 (11002)	4587 (4098)	3262 (2986)
B3LYP/AUG-cc-pVTZ	11421 (11124)	4526 (4046)	3241 (2967)
CCD/AUG-cc-pVDZ	11288 (11001)	4781 (4267)	3358 (3074)
MP2/6-311++G**	11233 (10941)	4831 (4319)	3381 (3101)
MP2/AUG-cc-pVDZ	11439 (11197)	4701 (4214)	3331 (3061)
CO_2–$(H_2O)_2$ and CO_2–$(D_2O)_2$			
Experiment[b]	6163 (5527)	2226 (2090)	1638 (1523)
RHF/6-311++G**	6177 (5507)	2151 (2009)	1601 (1479)
B3LYP/AUG-cc-pVDZ	6110 (5477)	2217 (2076)	1638 (1519)
B3LYP/AUG-cc-pVTZ	6029 (5421)	2223 (2080)	1639 (1520)
MP2/6-311++G**	6233 (5589)	2248 (2099)	1664 (1539)
MP2/AUG-cc-pVDZ	6217 (5567)	2250 (2106)	1663 (1541)

[a]Rotational constants of CO_2–D_2O and CO_2–$(D_2O)_2$ are given in parentheses
[b]From Ref [8,11]

at the corresponding levels of theory (Table 1) reveals that the binding energy per water molecule increases by about 1.3 times at the RHF/6-311++G** level, and by different factors lying between 1.7 and 2.2 at the higher levels of theory in going from CO_2–H_2O to CO_2–$(H_2O)_2$. The optimized distance between the carbon atom of $CO_2$and the oxygen atom of the water molecule bound to it also decreases at all the levels of calculations in going from CO_2–H_2O to CO_2–$(H_2O)_2$ (Tables 1, 3). The CO_2–$(H_2O)_2$ complex has a cyclic structure where one water molecule is bound to CO_2 as in CO_2–H_2O while the second water molecule is hydrogen bonded to both CO_2 and the first water molecule as follows (Fig. 1c). A hydrogen atom of the second water molecule is hydrogen bonded to an oxygen atom of CO_2 and its oxygen atom is hydrogen bonded to a hydrogen atom of the first water molecule (Fig. 1c), the two water molecules being in nearly mutually perpendicular planes, as is observed in a free water dimer [11,38,39]. Thus in CO_2–$(H_2O)_2$, while one water molecule would remain bound to CO_2 mainly through electrostatic interaction, the other water molecule, is bound to the first water molecule though a hydrogen bond, which in turn is bound to CO_2 through a hydrogen bond. Thus the water dimer is more strongly bound to CO_2 than a single water molecule, as shown by binding energies per water molecule. The water molecule that is bound to CO_2 mainly by electrostatic interaction in CO_2–$(H_2O)_2$ is not coplanar with CO_2. In this case, the O2C1O4H6 dihedral angle (Fig 1c) is about 35°. As shown by hydrogen bond lengths, the hydrogen bond between the two water molecules in CO_2–$(H_2O)_2$ (Fig. 1c) is stronger than that between an oxygen atom of $CO_2$and a hydrogen atom of a water molecule as well as that between the two water molecules of a free water dimer. In CO_2–$(H_2O)_2$, the two hydrogen bond lengths were found to be 1.92 and 2.19 Å respectively at the B3LYP/AUG-cc-pVDZ level of theory.

The calculated values of the dipole moments of CO_2–$(H_2O)_2$ by the different theoretical methods are in satisfactory

Table 3 Binding energy (BE) per water molecule, C–O(H_2O), O(CO_2)–O(H_2O) and O(H_2O)–O(H_2O) distances and dipole moments obtained by different methods for the CO_2–$(H_2O)_2$ complex

Method/Basis set	B.E per water molecule (eV)	C(CO_2)–O(H_2O) (Å)	O(CO_2)–O(H_2O) (Å)	O(H_2O)–O(H_2O) (Å)	Dipole Moment (Debye)
Experiment[a]		2.86	3.05	2.85	1.745
RHF/6-311++G**	−0.159	2.82	3.15	2.91	2.01
B3LYP/AUG-cc-pVDZ	−0.181	2.83	3.06	2.84	1.67
B3LYP/AUG-cc-pVTZ	−0.174	2.86	3.06	2.84	1.67
MP2/6-311++G**	−0.249	2.78	3.03	2.83	1.97
MP2/AUG-cc-pVDZ	−0.231	2.75	3.01	2.84	1.63

[a]From Ref. [11]

agreement with the experiment [11], the RHF/6-311++G** value is showing maximum disagreement (∼15%) and the B3LYP/AUG-cc-pVDZ and B3LYP/AUG-cc-pVTZ values are showing minimum disagreement (∼4%) (Table 3). The calculated principal rotational constants A, B and C of CO_2–$(H_2O)_2$ and CO_2–$(D_2O)_2$ are presented in Table 2, where these are compared with the experimental results due to Peterson et al. [11]. The percentage differences between the calculated and observed rotational constants of CO_2–$(H_2O)_2$ and CO_2–$(D_2O)_2$ are smaller (less than ∼1.5%) than the corresponding differences for CO_2–H_2O and CO_2–D_2O, excepting the results obtained at the RHF/6-311++G** and MP2/AUG-cc-pVDZ levels. The bending of CO_2in CO_2–$(H_2O)_2$is more prominent than that in CO_2–H_2O, lying in the range 2.6–2.9° according to the different calculations (Fig. 1c). Out of the two CO bonds of CO_2, in CO_2–$(H_2O)_2$, the one which is involved in hydrogen bonding with a water molecule is somewhat elongated (by ∼0.007 Å) while the other is shortened by a similar amount according to all the calculations. The OH bond lengths of the two water molecules that are involved in hydrogen bonding are elongated by ∼0.005 to ∼0.009 Å according to the different calculations, as compared to those that are not involved in hydrogen bonding. The HOH bond angles of both the water molecules are increased by ∼0.8 to 1.3° according to the different calculations. Further, increase in the OH bond length and HOH bond angle are larger for the water molecule that is bound to the carbon atom of CO_2 than those of the other water molecule. The assumption of no change in the geometries of CO_2 and water molecules in the experimental studies [11,12] appears to be more serious in CO_2–$(H_2O)_2$ than in CO_2–H_2O.

3.3 Structures, stabilities and properties of the CO_2–$(H_2O)_n$, (n = 3–8) complexes

Smallest CO(H_2O) distances between CO_2 and water molecules as well as binding energies per water molecule for the different CO_2-$(H_2O)_n$, (n = 3–8), complexes obtained at the B3LYP/AUG-cc-pVDZ level of theory are presented in Table 4 and the corresponding optimized structures are shown in Figs. 1d–f and 2a–c. We find that the smallest CO(H_2O) distance for $n = 5$ is the largest among all the CO(H_2O) distances while the reverse is true for the CO(H_2O) distance for $n = 7$. In going from $n = 2$ to 3 the binding energy per water molecule increases slightly, while in going to $n = 4$ and 5 it increases substantially. At $n = 6$, the binding energy per water molecule drops appreciably, but it again increases substantially when $n = 7$ and 8. If we consider variation of calculated dipole moments with n in the complexes CO_2–$(H_2O)_n$, (n = 3–8), we find a drop in the value of this property also for $n = 6$. The drop in the values of both binding energy per water molecule and dipole moment at $n = 6$ can be broadly understood in terms of structures as follows. In the complex for $n = 3$ (Fig. 1d), the plane of the middle water molecule, the oxygen atom of which is bound to the carbon atom of CO_2 is nearly perpendicular to those of the other two water molecules that are bound to CO_2 by one hydrogen bond each. The middle water and the CO_2 molecules are not coplanar and the structure of the complex for $n = 3$ is asymmetric. In going from $n = 3$ to 4 to 5 (Fig. 1d–f), structural asymmetry persists. In each of the two cases when $n = 4$ and 5, the oxygen atom of one water molecule is bound to the carbon atom of CO_2 while another water molecule is involved in a hydrogen bond with an oxygen atom of CO_2, and the water molecules are involved in a hydrogen bonded network.

The structures of the complexes CO_2–$(H_2O)_n$, (n = 6–8) are shown in Fig. 2a–c. For $n = 6$, the oxygen atoms of two water molecules are bound to the carbon atom of CO_2 while the other four water molecules are hydrogen bonded to CO_2 by a hydrogen bond each (Fig. 2a). In this case, almost the same structure as that obtained for $n = 3$ discussed above is present on the two opposite sides of CO_2 (Fig. 2a). For $n = 6$, the oxygen atoms of the middle water molecules (say O1 and O2) located on the two opposite sides of CO_2 and the carbon atom of CO_2 are not in a straight line; instead, the O1CO2 angle is about 144° the O1C and O2C distances being 2.821 Å each. A reflection plane passing through the CO_2 molecule is a symmetry element of this (n = 6) structure. In going from $n = 6$ to $n = 7$ and 8, the structural symmetry is lost and the hydrogen bonding between water molecules dominates over the binding between water molecules and CO_2. For each of $n = 7$ and 8, the oxygen atom of one water molecule is bound to the carbon atom of CO_2, and a hydrogen bond exists between CO_2 and another water molecule. The number of hydrogen bonds between $CO_2$and water molecules is largest for $n = 6$ among all the complexes. As the hydrogen bonding between two water molecules is stronger than that

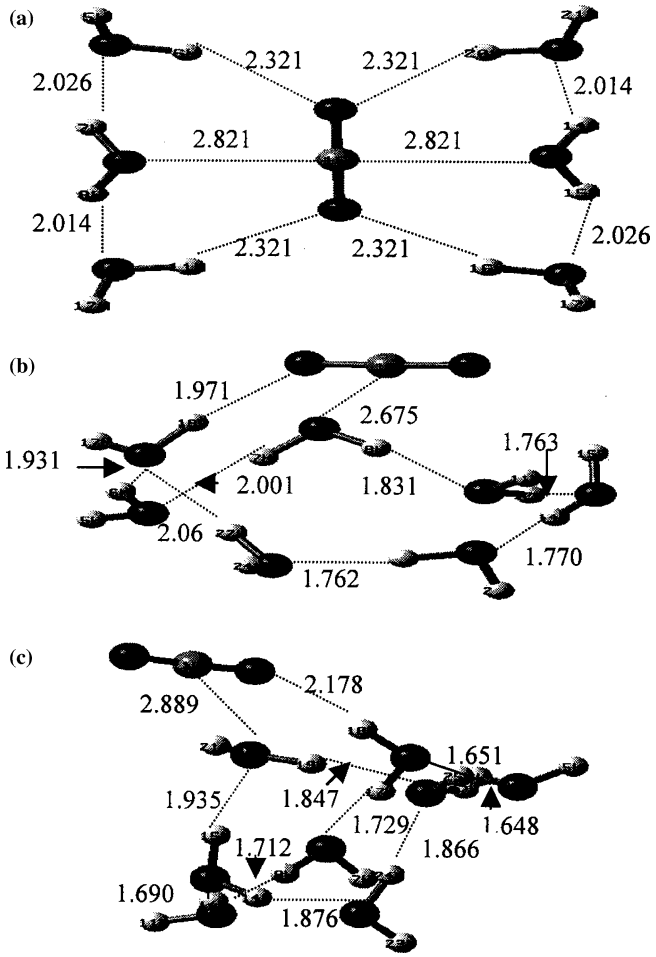

Fig. 2 Optimized structures of CO_2–$(H_2O)_n$, (n = 6–8), complexes are shown in (**a**), (**b**) and (**c**) respectively. All structures were optimized by the B3LYP/AUG-cc-pVDZ method

between a CO_2 and a water molecule, the optimized hydrogen bond lengths being ∼2.02 and 2.321 Å, respectively, at the B3LYP/AUG-cc-pVDZ level of theory, as discussed earlier, we can easily understand why the binding energy of CO_2–$(H_2O)_n$ for $n = 6$ per water molecule is lowest among the various cases (Table 4). Also, in view of its symmetry as discussed above, the complex for $n = 6$ has a lower dipole moment than those of the structures for $n = 4$, 5, 7 and 8.

Thus we find that the mode of binding between CO_2 and water molecules varies appreciably when n increases from 1 to 8. When n is greater than 3, except when $n = 6$, the water molecules prefer to make a hydrogen bonded network among themselves and keep CO_2 on the periphery of the network. Thus it seems that a solvation shell around CO_2 would involve a much larger number of water molecules than 8. A solvation shell around CO_2 consisting of 18 water molecules has been suggested using classical methods [40].

3.4 Rotational and reaction barriers

The rotational barrier heights of H_2O with respect to CO_2 in the CO_2–H_2O complex without and with ZPE correction as obtained by three different theoretical approaches are presented in Table 5. Attempts were made to calculate the barrier heights by the other methods given in Table 5 also, but these calculations were not successful and repeatedly got led astray. The differences between the calculated and observed rotational barrier heights lie within experimental error, excepting the B3LYP/AUG-cc-pVTZ value with ZPE correction that is somewhat less. In going from the equilibrium structure of the CO_2–H_2O complex to that corresponding to the rotational barrier (Fig. 3a) as obtained by the B3LYP-AUG-cc-pVTZ method, mainly the following two geometrical changes take place: (1) the O2C1O4H5 dihedral angle (Fig. 3a) is changed from 0° to 60° and (2) the CO(H_2O) distance between CO_2 and H_2O is increased by ∼0.2 Å. The other geometrical parameters of the system are changed by small amounts in this process.

The reaction between CO_2 and H_2O produces H_2CO_3. It is known from the previous studies [12–18] that this reaction is catalyzed by other water molecules of the aqueous medium, the effect of the second water molecule being most prominent. Further, it has been suggested that a strong rehybridization of atomic orbitals of the atoms involved in the reaction occurs at the transition state [18]. We undertook a study of this aspect for two reasons: (1) to study the rehybridization of orbitals at the transition states corresponding to one and two water molecules in detail, and (2) to investigate the barrier heights of the reactions with one and two water molecules using methods that take care of electron correlation to different extents including such methods and basis sets that are quite suitable for this purpose. Actually, the (2) part is related to the (1) part, as knowledge about reaction barrier is required for the study of rehybridization of atomic orbitals. The rehybridization aspect is discussed in the

Table 4 Smallest CO(H_2O) distances, binding energies per water molecule and dipole moments of $(CO_2$–$H_2O)_n$, n = 3–8, complexes obtained by the B3LYP/AUG-cc-pVDZ method

Number (n) of water molecules	Smallest CO(H_2O) distance (Å)	Binding energy per water molecule (eV)	Dipole moment (Debye)
3	2.732	−0.186	0.837
4	2.897	−0.245	2.325
5	3.070	−0.280	4.192
6	2.821	−0.176	1.235
7	2.675	−0.294	4.419
8	2.889	−0.340	3.400

Table 5 Rotational barrier of the CO_2–H_2O complex and reaction barrier for formation of H_2CO_3 and H_2CO_3–H_2O from CO_2–H_2O and CO_2–$(H_2O)_2$ respectively

Method/ Basis Set	Rotational barrier (kcal/mol)[a]	Reaction barrier (kcal/mol) for[b]	
		H_2CO_3	H_2CO_3-H_2O
Experiment[c]	0.9±0.2	17.7	
RHF/6-311++G**	1.0 (0.7)	70.2 (69.3)	49.0 (49.1)
B3LYP/AUG-cc-pVDZ		48.7 (48.0)	29.2 (28.4)
B3LYP/AUG-cc-pVTZ	0.7 (0.6)	50.1 (49.5)	
MP2/6-311++G**	0.9 (0.7)	55.6 (54.7)	38.0 (37.3)
MP2/AUG-cc-pVDZ		52.4 (51.4)	
CCD/AUG-cc-pVDZ		55.9 (55.2)	
MP2 (full)/6-31g**[d]		50.2	30.9
QCISD (T)/6-31G**//MP2 (full)/6-31G**[e]		50.6	31.8

[a]Rotational and reaction barriers with ZPE correction are given in parentheses
[b]Barrier height is given with respect to the total energy of the respective CO_2–H_2O or CO_2–$(H_2O)_2$ complex
[c]From Ref [8, 19]
[d]From Ref [18]
[e]Obtained by single-point calculation using the optimized geometry at the MP2 (full)/6-31G** method in Ref [18]

following subsection. The calculated reaction barrier heights with a single water molecule, without and with ZPE correction (Table 5), are found to be much higher than the experimental value (17.7 kcal/mole) [19]. The present calculated barrier height with a single water molecule at the MP2/6-311++G** level is lower by about 20% than that obtained at the RHF/6-311++G** level (Table 5). Obviously, inclusion of electron correlation lowers down the reaction barrier height appreciably. The barrier heights with a single water molecule obtained at the MP2/6-311++G** and CCD/AUG-cc-pVDZ levels of theory are very similar. The barrier height is reduced by 30–40% due to inclusion in the system of a second water molecule at the different levels of theory (Table 5). Thus the second water molecule plays a strong catalytic role in the reaction. The lowest barrier height was obtained in the present study with two water molecules at the B3LYP/AUG-cc-pVDZ level of theory as 28.4 kcal/mole (with ZPE).

The optimized structures of transition states of the above-mentioned reactions with one and two water molecules are shown in Figs 3b,c while the most stable conformations of the corresponding products H_2CO_3 and H_2CO_3–H_2O are shown in Fig. 3d,e, respectively. The structure of the transition state with a single water molecule (TS1W) (Fig. 3b) reveals the following information: (1) one OH bond of the water molecule remains almost unaffected while the other OH bond is broken, and the dissociated hydrogen atom is nearly equally distant (∼1.24 Å) from an oxygen atom of CO_2 and the oxygen atom of the water molecule, (2) the distance between the carbon atom of CO_2 and the oxygen atom of the water molecule (∼1.7 Å) is appreciably less than that in the equilibrium structure of the complex (∼2.8 Å), (3) one CO bond length of CO_2 is increased by about 0.1 Å while the other CO bond length is only slightly increased, and (4) the OCO bond angle of CO_2 is decreased by about 32°. When we consider two water molecules reacting with CO_2 leading to the formation of H_2CO_3–H_2O, the structure of the transition state (TS2W) is modified appreciably (Fig. 3c) as follows: (1) one OH bond length of each of the two water molecules remains almost unaffected, (2) one OH bond of one of the water molecules (first water molecule) is broken as in the reaction with one water molecule, and the dissociated hydrogen atom is shared by the oxygen atoms of both the water molecules, it being located much closer to the oxygen atom of the second water molecule than to that of the first, (3) one OH bond length of the second water molecule is elongated by about 0.1 Å, and the corresponding hydrogen atom is bound to an oxygen atom of CO_2, (4) at TS2W, the distance between the carbon atom of CO_2 and the oxygen atom of one of the water molecules (∼1.6 Å) is less than even the corresponding distance at TS1W (∼1.7 Å), (5) the CO bond length of CO_2 that was strongly elongated at TS1W is elongated to a somewhat smaller extent at TS2W, while the reverse is true for the other CO bond, and (6) the OCO bond angle of CO_2 is decreased further by about 6.5° at TS2W than that at TS1W. The structures of TS1W and TS2W obtained in the present study are broadly similar to those reported previously [14, 15, 18]. However, there are quantitative differences between the geometrical parameters obtained in the present and previous studies [14, 15, 18] for TS1W and TS2W due to the use of different theoretical methods.

3.5 Rehybridization of atomic orbitals

At transition states of reactions, atomic rearrangements on the potential energy hypersurfaces occur due to which rehybridization of atomic orbitals would take place. This interesting aspect of transition states of the reactions involved in the formation of H_2CO_3 and H_2CO_3–H_2O has been studied by Lewis and Glaser [18] using atomic site-based point charges obtained by natural population analysis (NPA) [41]. We have studied this aspect in much greater detail here using an approach that is particularly suitable in this context. The concept of HDC have been developed in our group both at semi-empirical and ab initio levels of theory [20–25]. Recently, a combination of bond-centered charges (BCC) with HDC was found to explain molecular properties satisfactorily [25]. In the present study, we have not included BCC as our aim here is

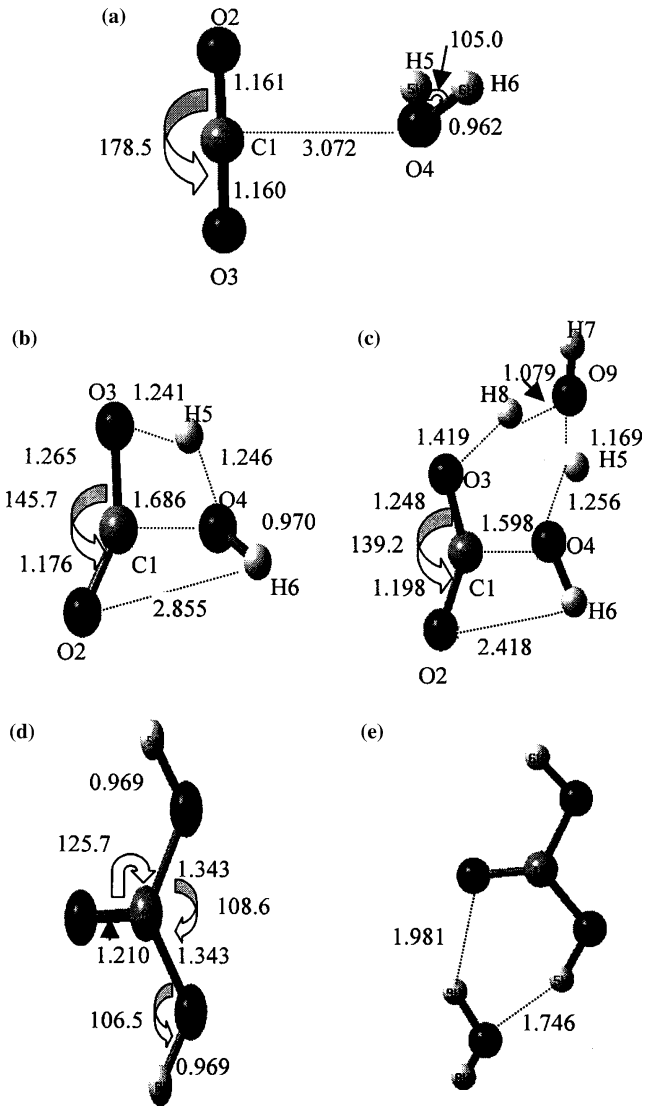

Fig. 3 **a** Structure of CO_2–H_2O complex at the rotational barrier, **b** structure of CO_2–H_2O complex at the reaction barrier leading to the formation of H_2CO_3, **c** like **b**, but with two water molecules, **d** optimized structures of H_2CO_3, **e** optimized structure of H_2CO_3–H_2O. In **a**, B3LYP/AUG-cc-pVTZ method was used while the B3LYP/AUG-cc-pVDZ method was used in the other cases

only to study rehybridization of atomic orbitals in going from equilibrium structures to transition states. Details of the methodology to compute HDC are available in the literature [20–25]. While the atomic site-based point charges, for example, Löwdin, Mulliken and NPA [42] do not even reproduce total molecular dipole moments, HDC preserve them satisfactorily [20–25]. Further, the contributions of different atoms to the component of total molecular dipole moment arising due to atomic orbital hybridization are also easily obtained using HDC. One can also calculate the individual HDC components arising due to mixing of specific atomic orbitals, for example, (ns, mp), where n and m are principal quantum numbers associated with the s and p types of orbitals of an atom. The following two approximations are involved in calculating HDC [23–25]: (1) Single point RHF/6-31G** calculations are carried out using B3LYP/AUG-cc-pVDZ optimized geometries. The density matrices obtained from RHF/6-31G** calculations are interpreted as having been computed using Slater type atomic orbitals. Further, the Slater exponents involved in HDC calculations have been so adjusted that they produce the best possible agreement between the molecular dipole moments obtained using SCF wave functions and HDC. (2) A parameter (K) involved in the HDC calculations is so adjusted that molecular electrostatic potentials near different atoms on the van der Waals surfaces in closest possible agreement with those computed using potential-derived atomic site-based point charges (e.g. CHelpG) [31] are obtained. The parameter K does not affect dipole moments. The RHF/6-31G** method was used in the HDC calculations since the necessary parameters (Slater exponents and K) were optimized at this level.

As HDC are displaced from atomic sites, a positive charge equal to the magnitude of total HDC is created at each atomic site. When this positive charge is added to the net positive or negative charge arising independently of HDC at the atomic site [43], we get the total atomic site charge (ASC). The calculated HDC components arising due to the mixing of atomic orbitals and their distances from the corresponding atoms as well as total HDC for different atoms in the equilibrium structures of CO_2–H_2O and CO_2–$(H_2O)_2$ and the corresponding transition states leading to the formation of H_2CO_3 and H_2CO_3–H_2O respectively, along with ASC, are presented in Table 6. Locations of HDC components associated with different atoms in the CO_2–$(H_2O)_2$complex, as an example, are shown in Fig. 4. The numbering scheme adopted here is explained in the caption to this figure. It may be remarked that the distances of HDC components from carbon, oxygen and hydrogen atoms are small but the corresponding distances for certain other types of atoms, particularly metal atoms, are quite appreciable [24, 25]. We find that the following changes take place in HDC magnitudes in going from the equilibrium structures of CO_2–H_2O and CO_2–$(H_2O)_2$ to the corresponding transition states (Figs. 1a,c, 3b,c and 4): (1) The magnitudes of some of the HDC components, for example, those arising due to (2s,2p) and (2s,3p) orbital mixing, and total HDC magnitudes, associated with C1 (Fig. 4) are strongly increased. It is a consequence of changes in the C1O2 and C1O3 bond lengths and O2C1O3 bond angle occurring in the process. (2) All the HDC magnitudes associated with both O2 and O3 decrease, it being more prominent for the latter atom than the former. It is easily understood since the C1O3 bond length is elongated more than the C1O2 bond length in the process under consideration. (3) The magnitudes of all the HDC components associated with O4 decrease following the process under consideration. It can be understood in view of the fact that a hydrogen atom bonded to O4 is getting dissociated in the reaction in both the systems. (4) HDC magnitudes associated with H5 are decreased appreciably while those associated with H6 are only slightly affected. Obviously, it arises due to the fact that H5 gets dissociated from O4 while H6 all along remains bonded to it. (5) The HDC magnitudes

Table 6 Hybridization displacement charges and atomic site charges (ASC) (in the unit of magnitude of electronic charge), associated with different atoms in the equilibrium structures of CO_2–H_2O and CO_2–$(H_2O)_2$ complexes and at the transition states involved in the formation of H_2CO_3 and H_2CO_3–H_2O, respectively, along with their distances from the corresponding atoms

Atom[a]	Mixing of orbitals	Amount of HDC[b]		Distance of HDC from the atom
		CO_2–H_2O	CO_2–$(H_2O)_2$	(Å)
C1	(1s, 2p)	−0.002(−0.025)	−0.003(−0.026)	0.114
	(2s, 2p)	−0.002(−0.198)	−0.012(−0.216)	0.040
	(1s, 3p)	−0.001(−0.029)	−0.002(−0.025)	0.073
	(2s, 3p)	−0.004(−0.181)	−0.016(−0.163)	0.021
	(3s, 2p)	−0.061(−0.137)	−0.058(−0.048)	0.021
	(3s, 3p)	−0.017(−0.104)	−0.011(−0.058)	0.022
	Total HDC	−0.086(−0.675)	−0.103(−0.537)	
	ASC	1.022(1.680)	1.056(1.561)	
O2	(1s, 2p)	−0.061(−0.057)	−0.061(−0.055)	0.114
	(2s, 2p)	−0.484(−0.465)	−0.491(−0.430)	0.040
	(1s, 3p)	−0.043(−0.039)	−0.043(−0.039)	0.073
	(2s, 3p)	−0.351(−0.331)	−0.350(−0.323)	0.021
	(3s, 2p)	−1.145(−1.023)	−1.160 (−1.009)	0.021
	(3s, 3p)	−0.680(−0.613)	−0.676(−0.621)	0.022
	Total HDC	−2.764(−2.528)	−2.780(−2.477)	
	ASC	2.292(2.046)	2.333(1.913)	
O3	(1s, 2p)	−0.061(−0.051)	−0.059(−0.048)	0.114
	(2s, 2p)	−0.485(−0.399)	−0.463(−0.387)	0.040
	(1s, 3p)	−0.043(−0.029)	−0.043(−0.032)	0.073
	(2s, 3p)	−0.351(−0.252)	−0.349(−0.278)	0.021
	(3s, 2p)	−1.144(−0.883)	−1.144(−0.848)	0.021
	(3s, 3p)	−0.679(−0.500)	−0.692(−0.526)	0.022
	Total HDC	−2.764(−2.114)	−2.750(−2.119)	
	ASC	2.293(1.476)	2.242(1.392)	
O4	(1s, 2p)	−0.054(−0.038)	−0.052 (−0.031)	0.114
	(2s, 2p)	−0.371(−0.327)	−0.344(−0.257)	0.040
	(1s, 3p)	−0.048(−0.036)	−0.047(−0.034)	0.073
	(2s, 3p)	−0.362(−0.288)	−0.342(−0.265)	0.021
	(3s, 2p)	−1.134(−0.740)	−1.090(−0.652)	0.021
	(3s, 3p)	−0.893(−0.618)	−0.867(−0.578)	0.022
	Total HDC	−2.862(−2.047)	−2.741(−1.817)	
	ASC	2.175(1.272)	2.000(1.013)	
H5	(1s, 3p)	−0.022(−0.010)	−0.023(−0.007)	0.082
	(2s, 3p)	−0.029(−0.008)	−0.023 (−0.000)	0.003
	Total HDC	−0.052(−0.018)	−0.046(−0.008)	
	ASC	0.398(0.530)	0.427(0.527)	
H6	(1s, 3p)	−0.022(−0.024)	−0.022(−0.024)	0.082
	(2s, 3p)	−0.029(−0.027)	−0.030(−0.026)	0.003
	Total HDC	−0.052(−0.051)	−0.052(−0.050)	
	ASC	0.398(0.428)	−0.389(0.432)	
H7	(1s, 3p)		−0.023(−0.024)	0.082
	(2s, 3p)		−0.029(−0.027)	0.003
	Total HDC		−0.052(−0.051)	
	ASC		0.400(0.431)	
H8	(1s, 3p)		−0.023(−0.013)	0.082
	(2s, 3p)		−0.026(−0.004)	0.003
	Total HDC		−0.048(−0.017)	
	ASC		0.428(0.527)	
O9	(1s, 2p)		−0.052(−0.037)	0.114
	(2s, 2p)		−0.370(−0.332)	0.040
	(1s, 3p)		−0.046(−0.032)	0.073
	(2s, 3p)		−0.354(−0.300)	0.021
	(3s, 2p)		−1.054(−0.612)	0.021
	(3s, 3p)		−0.827(−0.469)	0.022
	Total HDC		−2.703(−1.782)	
	ASC		1.999(1.060)	

[a]For atomic numbering, see Figs. 1a,c and 3b,c
[b]The HDC values at transition states are given in parentheses

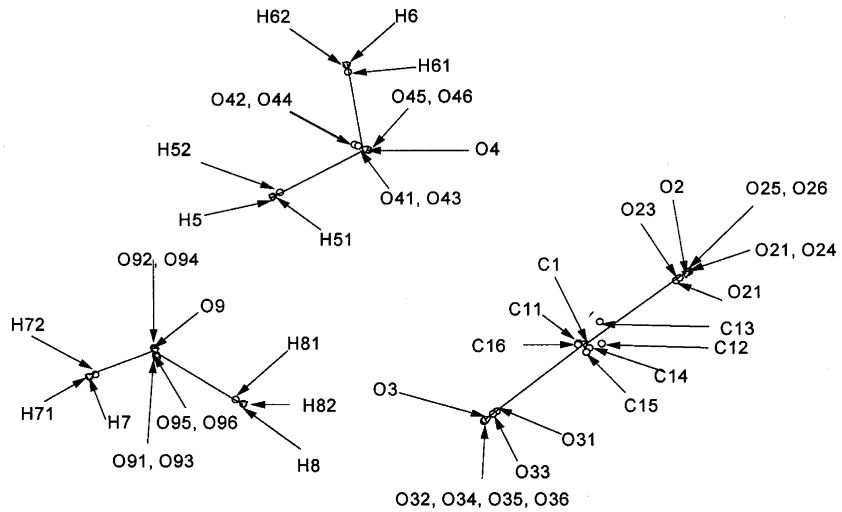

Fig. 4 Locations of HDC components in the equilibrium structure of CO_2–$(H_2O)_2$ complex. *Arrows* indicate locations of atoms (*open triangles*) and HDC components (*open circles*). The numbering scheme adopted here is as follows. The atoms (X) are numbered as Xi, (i = 1–9) while the HDC components for each i are numbered as Xij, where j = 1, 2 for hydrogen atoms and 1–6 for heavy atoms (C and O). The values of j for different HDC components associated with the heavy atoms are as follows: 1: (1s, 2p), 2: (2s, 2p), 3: (1s, 3p), 4: (2s, 3p), 5: (3s, 2p), 6: (3s, 3p), while for hydrogen atoms, these are as follows: 1: (1s, 3p), 2: (2s, 3p). In some cases, atomic locations and HDC components are overlapping

associated with H8 are decreased considerably while those associated with H7 are modified only slightly. It is a consequence of the fact that the O9H8 bond is appreciably elongated while the O9H7 bond length remains almost unaffected. (6) All the HDC magnitudes associated with O9 are decreased appreciably. It is a consequence of elongation of the O9H8 bond, while H5 is also located far away from it (Fig. 3c).

Thus except the HDC magnitudes associated with C1, those associated with all the other atoms decrease in going from the equilibrium structures to the corresponding transition states or are almost unaffected. The above discussion reveals that, in the present case, the total HDC magnitude associated with an atom is appreciably increased or decreased depending on whether its distances from other atoms are appreciably decreased or increased in comparison to the equilibrium values, including the situation when the bond under consideration is strongly elongated. Since the reactivity of an atom that is actively involved in a chemical reaction is increased at the transition state, it appears that the change of total HDC of an atom with respect to that in the equilibrium structure would be a measure of its reactivity. According to this criterion, reactivities of the atoms C1, O3, O4, H5 at TS1W (Fig. 3b) and C1, O3, O4, H5, H8, O9 at TS2W (Fig. 3c) would be appreciably enhanced in going from the equilibrium structures to the corresponding transition states. It appears to be quite acceptable as the above-mentioned atoms are directly involved in the reactions. Further, according to this criterion, the atoms O2, H6 at TS1W (Fig. 3b) and O2, H6, H7 at TS2W (Fig. 3c) would possess low reactivity. It is also quite acceptable as these atoms are not directly involved in the reactions. Generality of this criterion of reactivity expressed in terms of change of total HDC remains to be examined.

4 Conclusion

We arrive at the following conclusions from this study:

(1) Geometry optimization calculations using different methods performed in the present work suggest that the equilibrium structure of the CO_2–H_2O complex is symmetric, planar and so-called T-shaped, in agreement with the results obtained in previous studies. The same structure is also suggested experimentally on the basis of observed principal rotational constants and some assumptions. However, the present MP2/AUG-cc-pVDZ calculation predicts the structure to be unsymmetric, planar. Quantitative agreement between the observed principal rotational constants and the calculated ones using different methods argues in favor of the unsymmetric structure obtained by the MP2/AUG-cc-pVDZ method.

(2) The CO_2–H_2O complex is stabilized mainly by electrostatic interaction between the CO_2 and H_2O components and the contribution of van der Waals interaction in this case is much less.

(3) When the number of water molecules (n) is greater than 3, upto 8, except when n = 6, water molecules are involved in a hydrogen bonded network among themselves while CO_2 lies on the periphery of the network. It appears that a solvation shell around CO_2 would involve a much larger number of water molecules than 8.

(4) The calculated results show that electron correlation is important from the point of view of reaction barrier heights involved in the formation of H_2CO_3 and H_2CO_3–H_2O, but use of high-accuracy methods, for example, CCD in place of other methods, for example, MP2 and B3LYP, taking appropriate basis sets in all the cases, does not reduce the calculated barrier heights of the reactions, thus

not improving agreement with experiment. Thus electron correlation seems to plays a complex role in this context.

(5) Atomic orbitals are strongly rehybridized in going from the equilibrium structures of CO_2–H_2O and CO_2–$(H_2O)_2$ to the transition states involved in the formation of H_2CO_3 and H_2CO_3–H_2O, respectively, and HDC provide detailed information in this context. It appears that the change of total HDC of an atom of a molecule when the molecular geometry is distorted, for example, in going from the equilibrium structure to a transition state, would serve as a measure of its reactivity.

Acknowledgements The authors are thankful to Dr. A. K. Singh for help in the calculations of HDC. The authors are also thankful to the Council of Scientific and Industrial Research (New Delhi) and the University Grants Commission (New Delhi) for financial support.

References

1. Castaing M, Bursaux E, Poyart C (1982) Eur J Biochem 121:573
2. Gutt CN, Kim ZG, Hollander D, Bruttel T, Lorenz M (2001) Surg Endosc 15:314
3. Lehninger AL (1982) Principles of biochemistry. Worth Publishers, New York
4. Wullschleger SD, Tschaplinski TJ, Norby RJ (2002) Plant Cell Enviorn 25:319
5. Grunzweig JM, Korner C (2001) Oecology 128:319
6. Hirofumi S, Nobuyuki M, Masaru N, Fumio H (2000) Chem Phys Lett 323:257
7. Fredin L, Nelander B, Ribbegard G (1975) Chem Scr 7:11
8. Peterson KL, Klemperer W (1984) J Chem Phys 80:2439
9. Jönsson B, Karlstrom G, Wennerstrom H (1975) Chem Phys Lett 30:58
10. Tso T-L, Lee KC (1985) J Phy Chem 89:1612
11. Peterson KL, Suenram RD, Lovas FR (1991) J Chem Phys 94:106
12. Jönsson B, Karlstrom G, Wenerstrom H, Roos B (1976) Chem Phys Lett 41:317
13. Jönsson B, Karlstrom G, Wenerstrom H, Forsen S, Roos B (1977) J Am Soc 99:4628
14. Nguyen MT, Ha TK (1984) J Am Chem Soc 106:599
15. Nguyen MT, Hegarty AF, Ha TK (1987) J Mol Struct (Theochem) 150:319
16. Merz KM (1990) J Am Chem Soc 112:7973
17. Nguyen MT, Raspoet G, Vanquickenborne LG, Van Duijnem PT (1997) J Phys Chem A 101:7379
18. Lewis M, Glaser R (2003) J Phys Chem A 107:6814
19. Magid E, Turbec BO (1981) Biochim Biophys Acta 165:515
20. Mishra PC, Kumar A (1996) In: Murray JS, Sen KD (eds) Molecular electrostatic potentials: concepts and applications, theoretical and computational chemistry book series, vol 3. Elsevier, Amsterdam pp 257
21. Kumar A, Mohan CG, Mishra PC (1995) Int J Quant Chem 55:53
22. Singh AK, Kushwaha PS, Mishra PC (2001) Int J Quant Chem 82:299
23. Kumar A, Mishra PC (2001) J Mol Stuct (Theochem) 543:99
24. Singh AK, Mishra PC (2002) J Mol Struct (Theochem) 584:53
25. Singh AK, Kumar A, Mishra PC (2003) J Mol Struct (Theochem) 621:261
26. Head-Gordon M, Pople JA, Frisch MJ (1988) Chem Phys Lett 153:503
27. Kohn W, Sham LJ (1965) Phys Rev A 140:1133
28. Becke AD (1993) J Chem Phys 98:5648
29. Pople JA, Krishnan R, Schlegel HB, Binkley JS (1978) Int J Quant Chem 14:545
30. Woon DE, Jr Dunning TH (1993) J Chem Phys 98:1358
31. Breneman CM, Wiberg KB (1990) J Com Chem 11:361
32. Frisch AE, Nielsen AB, Holder AJ (2000) GaussView, Rev. 2.1, Gaussian Inc., Pittsburg
33. Frisch AE, Dennington RD, Keith TA, Nielsen AB, Holder AJ (2003) GaussView, Rev. 3.9, Gaussian Inc., Pittsburg
34. Frisch MJ, Trucks GW, Schlegel HB, Gill PMW, Johnson BG, Robb MA, Cheeseman JR, Keith T, Petersson GA, Montgomery JA, Raghavachari K, Al-Laham MA, Zakrzewski VG, Ortiz JV, Foresman JB, Peng CY, Ayala PY, Chen, Wong MW, Andres JL, Replogle ES, Gomperts R, Martin RL, Fox DJ, Binkley JS, Defrees DJ, Baker J, Stewart JP, Head-Gordon M, Gonzalez C, Pople JA (1995) Gaussian 94W, Revision E.3, Gaussian, Inc., Pittsburgh
35. Frisch MJ, Trucks GW, Schlegel HB, Scuseria GE, Robb MA, Cheeseman JR, Zakrzewski VG, Montgomery JA Jr, Stratmann RE, Burant JC, Dapprich S, Millam JM, Daniels AD, Kudin KN, Strain MC, Farkas O, Tomasi J, Barone V, Cossi M, Cammi R, Mennucci B, Pomelli C, Adamo C, Clifford S, Ochterski J, Petersson GA, Ayala PY, Cui Q, Morokuma K, Rega N, Salvador P, Dannenberg JJ, Malick DK, Rabuck AD, Raghavachari K, Foresman JB, Cioslowski J, Ortiz JV, Baboul AG, Stefanov BB, Liu G, Liashenko A, Piskorz P, Komaromi I, Gomperts R, Martin RL, Fox DJ, Keith T, Al-Laham MA, Peng CY, Nanayakkara A, Challacombe M, Gill PMW, Johnson B, Chen W, Wong MW, Andres JL, Gonzalez C, Head-Gordon M, Replogle ES, Pople JA (1998) Gaussian 98W, Revision A.11.2, Gaussian, Inc., Pittsburgh
36. Frisch MJ, Trucks GW, Schlegel HB, Scuseria GE, Robb MA, Cheeseman JR, Zakrzewski VG, Montgomery JA Jr, Stratmann RE, Montegomery JA Jr, Vreven T, Kudin KN Burant JC, Millam JM, Lyengar SS, Thomasi J, Barone V, Mennucci B, Cossi M, Schalmani G, Rega N, Petersson GA, Nakatsuji H, Hada M, Ehara M, Toyota K, Fukuda R, Hasegawa J, Ishida M, Nakajima T, Honda Y, Kitao O, Nakai H, Klene M, Li X, Knox JE, Hratchain HP, Cross JB, Adamo C, Jaramillo J, Ayala PY, Morokuma K, Voth GA, Salvador PS, Dannenberg JJ, Zakrzewski VG, Dapprich S, Daniels AD, Strain MC, Farkas O, Malick DK, Rabuck AD, Raghavachari K, Foresman JB, Ortiz JV, Cui Q, Baboul AG, Cliffered S, Cioslowski J, Stefanov BB, Liu G, Liashenko A, Piskorz P, Komaromi I, Martin RL, Fox DJ, Keith T, Al-Laham MA, Peng CY, Nanaykkara A, Challacombe M, Gill PMW, JohnsonB, ChenW, Wong MW, Gonzalez C, Pople JA (2003) Gaussian 03W, Revision B.05, Gaussian, Inc., Pittsburgh
37. Zhang NR, Shillady DD (1994) J Chem Phys 100:5230
38. Upadhyay DM, Shukla MK, Mishra PC (2001) Int J Quant Chem 81:90
39. Liu K, Brown MG, Carter C, Saykally RJ, Gregory JK, Clary DC (1996) Nature 381:501
40. Anderson GK (2003) J Chem Thermodyn 35:1171
41. Reed AE, Weinstock R, Weinhold F (1985) J Chem Phys 83:735
42. Jug K, Maksic ZB (1991). In: Maksic ZB (ed) Theoretical models of chemical bonding, Part III: molecular spectroscopy, electronic structure and intermolecular interaction,. Springer, Berlin Heidelberg New York p 235
43. Pople JA, Beveridge DL (1970) Approximate molecular orbital theory, McGraw-Hill, NewYork